Anomalous transport properties of a linear-chain metal: $NbSe_3$†

N. P. Ong
Department of Physics, University of California, Berkeley, California 94720
*and Department of Physics, University of Southern California, Los Angeles, California 90007**

Pierre Monceau‡
Department of Physics, University of California, Berkeley, California 94720
(Received 31 May 1977)

The transport properties of the linear-chain metal $NbSe_3$ are anomalous. Giant increases in the dc resistivity appear at 145 and 59 K, suggestive of charge-density-wave (CDW) formation. These anomalies show breakdown effects with applied electric fields as low as 0.1 $V cm^{-1}$. The temperature dependence of the resistivity also shows strong variation at microwave frequencies. We report measurements on the temperature dependence of the non-Ohmic effect together with microwave results and review the evidence for CDW formation. On the basis of the CDW model we have extracted a parameter α from the data which gives the fraction of the Fermi surface destroyed by the CDW gap. Other models are discussed and compared with the CDW model. We consider the possibility that the anomalous conductivity may arise from nonlinear excitations of a pinned CDW.

I. INTRODUCTION

The study of systems of restricted dimensionality has become an active area of research in the last few years. A general characteristic of two-dimensional and one-dimensional solids appears to be their instability toward the formation of charge-density-wave (CDW) states,[1] in which the electron gas and the lattice condense into a superlattice structure which may be detected by x-ray and neutron scattering or electron diffraction. In the one-dimensional metals[2] the CDWs (Peierls distortion[3]) have a wave vector $q = 2k_F$ in the chain direction, where k_F is the Fermi wave vector, and their formation drives the system into a semiconducting state (Peierls transition). In systems of higher dimensionality the onset of CDWs has less drastic effect on the transport properties and usually results in small anomalies in the resistivity. The existence of CDWs has been established experimentally in the layered compounds[4] (transition-metal dichalcogenides such as $2H$-$NbSe_2$ and $2H$-TaS_2) and the pseudo-one-dimensional metals, $K_2Pt(CN)_4Br_{0.3} \cdot 3H_2O$ (or KCP)[5] and tetrathiafulvalenium tetracyanoquinodimethanide (TTF-TCNQ).[6,7]

Recently, much interest has been shown in the transport properties of CDW systems. The possibility of either depinning an immobile CDW by high electric fields or creating current-carrying excitations (such as phase or amplitude solitons) has been theoretically discussed by several workers. If experimentally observed, such cooperative phenomena would present another example of many-body effects dominating transport properties in condensed matter.

Non-Ohmic conductivity (nonlinear I-V characteristic) has been reported in TTF-TCNQ[8] and in the recently synthesized polychalcogenide $NbSe_3$.[9] Although the non-Ohmicity in TTF-TCNQ has been interpreted[8] in terms of soliton creation, the data is also consistent with a single-particle hot-electron model and the exact interpretation is still a point of controversy. In this paper we report on the anomalous transport properties of $NbSe_3$. The preliminary results have been published elsewhere.[9,10] Here we describe the measurements in detail and present new evidence for many-body effects in the transport properties.

$NbSe_3$ crystallizes in fibrous strands in contrast to the layered structure of the dichalcogenides. The x-ray structure[11] [Fig. 1(a)] shows the formation of chains composed of trigonal prisms stacked end-to-end. Each prism consists of a Nb atom in the center with Se atoms at the vertices. Unlike the case in $2H$-$NbSe_2$ where neighboring prisms are in contact (i.e., Se atoms are shared), the adjacent chains in $NbSe_3$ are set apart. Six of these chains form the large unit cell. The Nb atoms in three of these chains are displaced a half lattice spacing in the b (chain) direction with respect to the Nb atoms in the other three chains. The formation of these chains suggests that quasi-one-dimensional band structure may result. Although the fibrous morphology has thus far precluded effective dc measurements on the transverse conductivity, microwave measurements on helical samples (Sec. II) indicate that the conductivity is highly anisotropic. However, recent Shubnikov-de Haas measurements[12] reveal strong oscillations with a single Fourier component at liquid-helium temperatures. The angular dependence

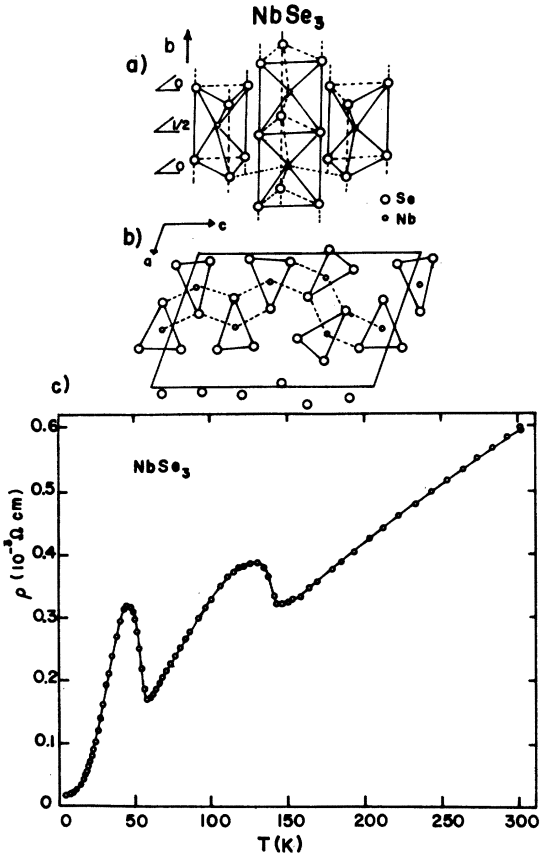

FIG. 1. (a) Crystal structure of $NbSe_3$ along the b axis. The Nb atoms in adjacent chains are displaced by half a lattice spacing along $\vec{b}$ with respect to each other. (b) Crystal structure of $NbSe_3$ in the a-c plane. The unit cell, comprised of six prisms and represented by the parallelogram, has the dimensions $a = 10.006$ Å, $b = 3.478$ Å, $c = 15.626$ Å, $\beta = 109.30°$. The Nb-Nb distance along $\vec{b}$ is 3.478 Å (compared to 2.68 Å in the metal). In the other directions it varies from 4.45 to 4.25 Å. The dashed lines connect Nb and Se atoms in the same plane. (c) Resistivity of $NbSe_3$ vs temperature. The phase transitions at 145 K and 59 K have been tentatively identified with the formation of charge-density waves.

of the oscillations indicates a cylindrical Fermi surface (FS) of surprisingly simply geometry.

Early measurements[13] [Fig. 1(c)] on the dc longitudinal resistivity showed metallic behavior down to 1 K. However, two giant anomalies which are indicative of phase transitions appear in the resistivity curve at 145 and 59 K. These anomalies are reminiscent of the resistivity anomalies which appear at the CDW transitions in the 2H-polytype layered compounds, as well as the anomaly in Cr at the spin-density-wave (SDW) transition.[14]

Further study[15] of the anomalies in $NbSe_3$ showed that both transition temperatures T_1 (145 K) and T_2 (59 K) decrease with pressure at the rate of 4K/kbars. A reduction in the anomaly amplitudes is also observed. At a pressure of 6 kbars the size of the lower-temperature anomaly is reduced by 90% compared to the ambient pressure result. The 59-K transition also shows a large thermal anomaly in the specific heat.[16] (The preliminary specific-heat measurements at 145 K do not have the sensitivity to detect any anomaly at the higher-temperature transition.) No evidence of superconductivity has been obtained at ambient pressure down to 50 mK. However, under pressure the metal becomes superconducting,[17] and T_c increases rather rapidly with pressure (0.6 K/kbars) before saturating. (At 5 kbars T_c is 2 K.) Because of the similarity of the above results to the well-studied case of 2H-$NbSe_2$, we have tentatively identified the transitions at T_1 and T_2 in $NbSe_3$ with CDW formation.[9,16] The arguments are reviewed in Sec. IV, and a new observation based on this hypothesis, which turns out to be consistent with experiment, is presented. X-ray measurements to look for superlattice formation are currently under way.

The most striking transport properties of $NbSe_3$ are the highly non-Ohmic dc conductivity[9] and the anomalous behavior of the conductivity at microwave frequencies.[10] These constitute the main topics of discussion in this paper. Electric field breakdown effects become apparent within the resistivity anomalies at fields as weak as 0.1 V cm^{-1}. The conductivity increases with electric field approximately as

$$\sigma(E, T) = \sigma_a(T) + \sigma_b(T) e^{-E_0(T)/E} , \tag{1}$$

where σ_a and σ_b are field-independent parameters, T is the temperature, and E is the applied field. We shall call the quantity E_0 the activation field. By measuring σ as a function of E at each temperature below T_1 we obtain the temperature variation of the three quantities σ_a, σ_b, and E_0. These results, which are presented in Sec. III, provide useful clues to the non-Ohmic mechanism and the nature of the transitions. In particular in the limits of low and high fields we have from Eq. (1):

$$\sigma(E \to 0) = \sigma_a , \tag{2}$$

$$\sigma(E \to \infty) = \sigma_a + \sigma_b . \tag{3}$$

We may define a parameter $\alpha(T)$ as

$$\alpha(T) = \sigma_b(T) / [\sigma_a(T) + \sigma_b(T)] . \tag{4}$$

α may be interpreted as a measure of the component of the conductivity which is non-Ohmic. Its physical significance is discussed in Sec. IV.

The resistivity of $NbSe_3$ has also been measured

at microwave frequencies by a cavity perturbation technique. At 9.3 GHz the amplitude of the 145-K anomaly is greatly suppressed. No trace of the 59-K anomaly is apparent at 9.3 GHz. The results are difficult to understand in a single quasiparticle picture. The simple Drude expression for the ac conductivity deviates significantly from the dc value only when $\omega\tau \gtrsim 1$. At 9.3 GHz this condition implies carrier lifetimes approaching 10^{-9} sec, which is several orders of magnitude longer than carrier lifetimes in say, semimetals (10^{-12} to 10^{-13} sec) at moderate temperature. The anomalous frequency dependence of the conductivity suggests that many-body effects may be dominating the transport properties below the transition temperatures. We will discuss in detail the evidence for such effects, as well as other possible causes, in Sec. IV.

II. EXPERIMENTAL TECHNIQUES

Measurements were done on two batches of samples. The first batch was synthesized at the Laboratoire de Chimie Minerale by J. Rouxel and co-workers, and the second batch was grown by J. Savage at the University of Southern California. Both batches were synthesized[11] by the direct reaction of Nb and Se in stoichiometric proportions inside a quartz tube. The tube was maintained at 750 °C for three to four weeks. Typical sample sizes for these experiments are $10 \times 0.02 \times 0.01$ mm^3.

For the dc and pulsed current measurements two kinds of cryogenic systems were used. The preliminary work was carried out in a continuous gas-flow cryostat. More precise measurements were subsequently carried out in a conventional Janis double-wall Dewar, which had a thermal stability of 20 mK/hr throughout the whole temperature range. The gas-flow system had superior thermal load, but had poorer stability and a larger temperature uncertainty. In the Janis system the temperature was monitored by a silicon thermal sensor and controlled by a commercial temperature controller. All microwave measurements were carried out in the gas-flow cryostat.

In the dc and pulsed-current measurements, gold leads were attached to the samples with silver paint (DuPont 4922, in butyl acetate solvent). Contact resistance was estimated to be less than 0.5 Ω for each lead. Ohmicity of the contacts was tested at room temperature up to the highest electric fields used. The current direction was also reversed to check the possibility of rectifying junctions forming between the silver paint and the sample. No differences resulting from the current direction were detected. On a freshly mounted sample a heavy pulsed current often decreased the resistance irreversibly. The new sample resistance (above 145 K) showed Ohmic behavior and good reproducibility as long as the current was kept below that of the initial pulse. This irreversible lowering of the sample resistance is frequently encountered in experiments using silver paint for lead attachments and is generally ascribed to an improvement in the paint conductance as a result of the passage of a heavy current. For the non-Ohmic experiments, resistivity in the low-field limit was measured with a dc current of 20 μA. Higher current values were pulsed with a duty cycle of 10^{-4} (pulse width ~2 μsec). The maximum power dissipation in the sample was estimated to be 7 μW. Sample heating led to a strong deviation from Eq. (1) when $\ln(\sigma - \sigma_a)$ was plotted against $1/E$.

Pulsed current was determined by measuring the voltage drop across a precision 100-Ω resistor in series with the sample. To measure the pulse heights to the level of accuracy (1 part in 10^4) required to test Eq. (1), the pulses were first passed through a bucking box designed to subtract a continuous adjustable constant value V from the pulse height. From the bucking box the pulses were displayed in a storage oscilloscope using a differential amplifier plug-in.

In the longitudinal microwave measurements[18] the sample was held in place inside a quartz sample tube by a polystyrene pad, with the sample b axis parallel to the rf electric field. The sample tube was filled with He gas and sealed. Cooling of the sample tube was achieved by the flow of the gas through a finger dewar that penetrated the cavity. At room temperature the sample could be moved in and out of the cavity to determine the frequency shift as well as the change in Q of the cavity. Frequency shifts were measured by introducing frequency markers on the transmission spectrum of the cavity through a beat-frequency klystron. The uncertainty in frequency shift measurement was 50 kHz. The transmitted signal was monitored by superheterodyne detection, and relative changes in Q of 1 part in 10^6 could be determined by phase-locking the main oscillator to the harmonic of a quartz crystal and measuring the change in transmitted power at the resonance frequency of the cavity. However, to determine the *absolute* change in Q the sensitivity decreased to 1 in 10^4 because spurious losses from other sources were of this order of magnitude. Typically a sample of dimensions $5.5 \times 0.035 \times 0.010$ mm^3 with a longitudinal depolarization factor N_b equal to 7.5×10^{-5} [Système International (SI) units] produced a frequency shift of -4.21×10^{-3} and a change in Q given by $\Delta(1/Q) = 4.77 \times 10^{-4}$. Since the bulk conductivity

from dc measurements corresponds to a value for ϵ_b'' (imaginary part of the dielectric constant in the longitudinal direction equal to $\sigma/\omega\epsilon_0$) in excess of 3.4×10^5 at room temperature, and increasing at lower temperatures, we have $N_b\epsilon_b'' \simeq 25 \gg 1$. In the cavity perturbation treatment[19-21] we are in the highly depolarized regime in which the frequency shift and loss are given by the equations

$$-\Delta\omega/\omega = \eta/N_b \ , \tag{5}$$

$$\Delta(1/Q) = (\eta/N_b)(1/N_b\epsilon_b'') \ , \tag{6}$$

where η is the filling factor of the sample. In agreement with Eq. (5) no temperature variation of $\Delta\omega/\omega$ was detected to the accuracy of the measurements even though the loss changed by a factor of 40. Equation (5) implies that the frequency shift is determined solely by sample geometry,[21] while Eq. (6) predicts that the loss is proportional to the bulk resistivity ρ_b along the longitudinal axis of the sample. No information on the real part of the dielectric constant can be obtained in this regime. To obtain a value for the absolute resistivity, Eq. (5) may be used in Eq. (6) to eliminate η/N. The greatest uncertainty comes from measuring c, the smallest dimension which appears in N_b. Since the same quantity must be measured to determine the dc bulk resistivity, the uncertainties in the 9.3-GHz absolute measurement of ρ_b is comparable to that at dc. The average of three samples at room temperature is 810 $\mu\Omega$ cm which is in reasonable agreement with the reported[13] dc value 600 $\mu\Omega$ cm.

In the regime where Eqs. (5) and (6) are valid the rf fields are assumed uniform inside the sample although substantially reduced through screening by free carriers. For this assumption to be valid the skin depth must be larger than or comparable to the smallest sample dimension. At 8 K the computed microwave resistivity is 15 $\mu\Omega$ cm, which corresponds to a skin depth of 6 μm. Since the smallest dimension of typical samples is 10 $\pm$4 μm, it is reasonable to assume that Eqs. (5) and (6) are valid throughout the temperature range investigated. Furthermore, in the skin-depth regime the loss is expected[22] to vary as $\Delta(1/Q)\sim(\rho_b)^{1/2}$. Comparison of the measured loss and the dc resistivity appropriately scaled to agree at high temperature would show the loss becoming proportionately larger as ρ_b decreases with temperature [if the loss goes as $(\rho_b)^{1/2}$]. However, as shown in Fig. 2, this is not the case. (Cohen *et al.*[22] have proposed an equation to treat loss in needle-shaped samples in the skin-depth regime, and applied it to measurements on TTF-TCNQ.) The large losses shown by some of the $NbSe_3$ samples at room temperature drop the Q by 50%, and the incident power has to be substantially reduced to avoid sample heating. Typical runs were made with 3-μW incident power. In some runs this was reduced to 300 nW with no detectable change in temperature variation of the measured loss. The cryogenics introduced a sample temperature uncertainty of $\pm$2 K because of the unavoidable thermal gradient in gas-flow cryostats. To minimize this uncertainty dc samples of $NbSe_3$ were used both upstream and downstream from the sample as thermometers. An attempt was made to measure the microwave loss and dc resistivity on the same sample, but this failed because of high radiation losses induced by the dc leads. Altogether, longitudinal measurements were made on eight samples with no significant disagreement.

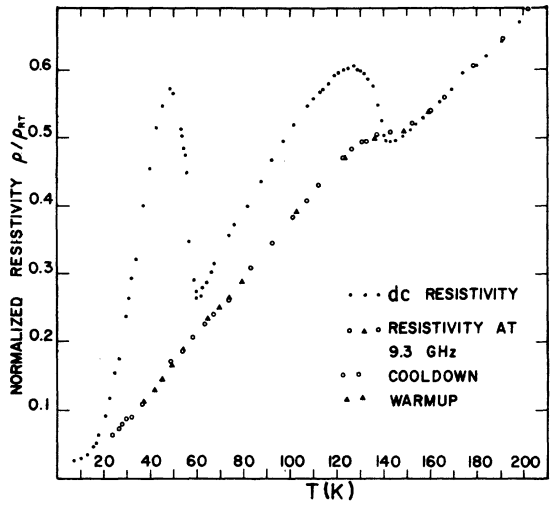

FIG. 2. Resistivity at 9.3 GHz compared to the dc resistivity as a function of temperature. Only one vertical scale adjustment has been made to bring the two sets of data into agreement at temperatures above 145 K. In the highly depolarized treatment used to analyze the microwave loss data the resistivity is directly proportional to the loss $\Delta(1/Q)$. The lower-temperature anomaly is completely suppressed while the high-temperature anomaly is greatly reduced.

The transverse resistivity cannot be reliably measured on a single fiber from the change in Q of the cavity mode in which the electric field is perpendicular to the chain direction. (We used a bimodal cavity[18] in which the two modes had their electric field respectively parallel and perpendicular to the sample axis.) The loss in the transverse direction for a single fiber was of the order of 1 in 10^4 (expressed as a relative change in Q). To increase the loss, a configuration[23] unique to the fibrous nature of the material was adopted. With vacuum grease as adhesive, approximately ten samples were wound around a thin-walled capillary tube (0.5-mm o.d.) to form a helical coil of dimensions $a=500$ μm, $b=300$ μm, $t=100$ μm.

The loss and frequency shift in the mode in which the electric field was parallel to the coil axis was measured. Typically in this configuration $|\Delta\omega/\omega| \sim 2.32\times10^{-4}$ and $\Delta(1/Q)\sim 3.39\times10^{-5}$. To extract a value for the transverse resistivity it was assumed that losses were predominantly due to electron transport perpendicular to the strands, the longitudinal loss being negligible because the rf electric field is perpendicular to the chains. This assumption would be invalid if the pitch of the windings was so large that a significant component of the rf field was along the chains. However, microscopic examination of the coil showed that the pitch angle was smaller than 0.5°, i.e., the longitudinal conduction was reduced by a factor of 10^{-4} compared to the transverse. The depolarization factor in this configuration may be obtained as the difference of that of two concentric cylinders whose radii differ by the small dimension t equal to the thickness of the winding. Thus if N is the longitudinal depolarization factor for a prolate spheroid of length $2a$ and maximum radius b, then the depolarization factor N_H for a helix is

$$N_H = N(m) - N(m+\delta m)\,, \tag{7}$$

$$N(m) = \frac{1}{m^2-1}\left(\frac{m}{(m^2-1)^{1/2}}\ln[m+(m^2-1)^{1/2}]-1\right), \tag{8}$$

$$m = a/b\,, \quad \Delta m \simeq tb/m\,. \tag{9}$$

For the helices used N_H is about 5.5×10^{-2}.

Using Eq. (7) in Eqs. (5) and (6) we get an estimate for the transverse resistivity. From measurements at room temperature on two helices the calculated transverse resistivity was 3.8 $(\Omega\ \mathrm{cm})^{-1}$ and 1.3 $(\Omega\ \mathrm{cm})^{-1}$. The discrepancy is not serious in view of the difficulty in estimating the smallest dimension t and errors introduced by nonuniformity in the windings. This corresponds to an anisotropy at room temperature of between 330 and 1200 [assuming a longitudinal conductivity of between 1300 and 1700 $(\Omega\ \mathrm{cm})^{-1}$]. These numbers for the anisotropy should be taken with caution because the geometry employed in the measurements on the helical samples does not lend itself to an unambiguous interpretation of the observed loss. For example, losses may be due to induced eddy currents flowing parallel to the windings.

III. EXPERIMENTAL RESULTS

Figures 3 and 4 show the plot of the dc conductivity $\ln(\sigma-\sigma_a)$ vs $1/E$ at various temperatures. The linear fit is good at all temperatures, demonstrating that Eq. (1) is valid at all temperatures below 145 K. The slope and intercept at each temperature give two numbers, from which E_0 and σ_b may be calculated, respectively. E_{01} and E_{02}

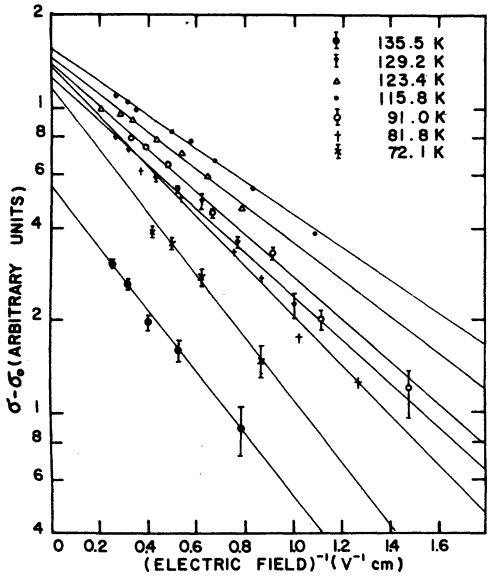

FIG. 3. Semilog plot of $\sigma-\sigma_{a1}$ vs $1/E$ for temperatures above 59 K. The straight lines indicate the behavior described by Eq. (1). The error bars represent the total uncertainty from both pulsed voltage and current measurements.

are shown as functions of temperature in Fig. 5. (Hereafter, second subscripts 1 and 2 refer to quantities associated with the 145 K and 59 K transitions, respectively. Quantities without second subscripts refer to the whole temperature range below 145 K without specific reference to either transition.) They appear to diverge as the temperature approaches the transition temperatures from below. As the temperature decreases, both E_{01} and E_{02} pass through a minimum (at temperatures a little higher than the temperatures where the low-field resistivity peaks), and then they increase rapidly. This nonmonotonic behavior is apparent on studying the constant current contours of Figs. 1 and 2 of Ref. 9. There it is clear that a higher current density is required to induce non-Ohmic behavior as the transition temperatures are approached from below. The minimum value of E_{01} is about an order of magnitude larger than that of E_{02}.

The prefactors of the field-dependent component of the conductivity within the high- and low-temperature anomaly σ_{b1} and σ_{b2} are shown as a function of temperature in Fig. 6. The information contained in E_0 and σ_b are quite independent of each other. The temperature dependence of E_0 is closely related to the dynamics of the mechanism that is responsible for the non-Ohmic behavior. Thus in any model of the nonlinear conducting mechanism E_0 can be expressed in terms of order parameters of the model, and the calculated temperature dependence may be compared

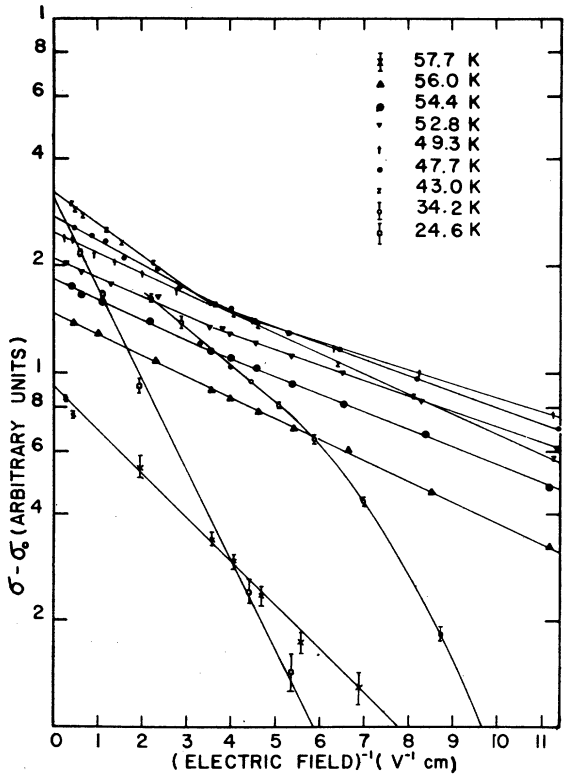

FIG. 4. Semilog plot of $\sigma - \sigma_{a2}$ vs $1/E$ for temperatures below 59 K. The steep slope of the 24.6-K line indicates the rapidly increasing value of E_{02} as the temperature decreases below 48 K. The deviation from linearity of the 34.2-K line arises from temperature instability during the measurements.

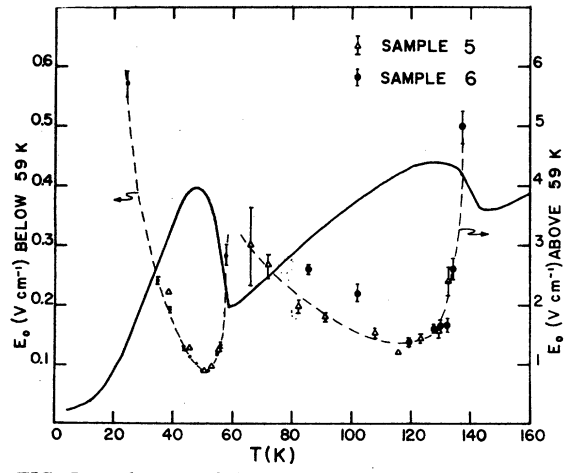

FIG. 5. Behavior of the activation field E_0 [as defined in Eq. (1)] vs temperature. The solid line is the low current resistivity while the dashed line is the best fit to the experimental data on E_0. The vertical scale below 59 K has been magnified by a factor of 10 compared to that above 59 K. Data from Samples 5 and 6 are shown together, with only one scale adjustment to make them agree at 50 K. (These samples are not listed in Table I.)

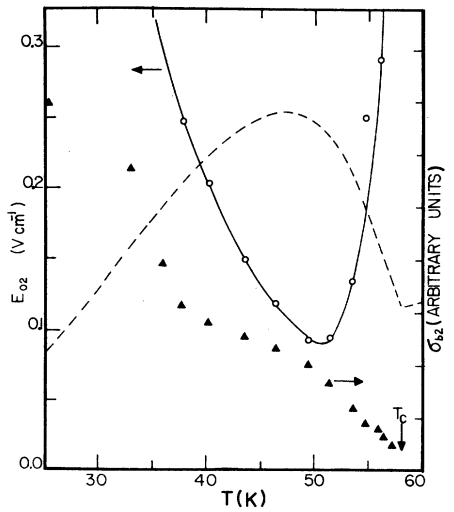

FIG. 6. Behavior of E_{02} and σ_{b2} vs temperature T below 59 K. E_{02} is extracted from the slope of the straight lines in Fig. 4, while σ_{b2} is obtained from the intercept of the lines with the y axis. As T decreases from 59 K, E_{02} (open circles) passes through a minimum and then increases rapidly. The prefactor σ_{b2} of the field-dependent part of the (solid triangles) increases monotonically with decreasing T. The low-field resistivity (broken line) is presented for comparison.

with the data in Fig. 5. On the other hand, σ_b is obtained by extrapolating the breakdown data to infinite field. As suggested by Eq. (3), σ_b within each anomaly provides a measure of the decrease in carriers that results from processes which set in at the phase transition. The application of high electric fields partially restores this loss, and in the limit of infinite fields the original carrier concentration is recovered. The temperature variation of σ_b then provides information on the fractional loss of carriers. This interpretation should be independent of the specific model used to explain the E_0 data. In Sec. IV we will relate σ_b to the destruction of FS area by CDW gaps.

The microwave resistivity profile at 9.3 GHz is compared with the low-field dc resistivity in Fig. 2. Both resistivities were measured in the longitudinal (b) direction on different samples. Only one vertical scale adjustment has been made to make both sets of data agree at temperatures above 145 K. In the microwave experiment there is a temperature uncertainty of 2 K arising from the thermal gradient between the sample and thermometer. The 9.3-GHz data show the presence of a small anomaly at 145 K but no trace of an anomaly at 59 K to the accuracy of the measurements. Readings were taken during cooling and warming with no observable hysteresis. A separate run was made with the empty cavity to determine the

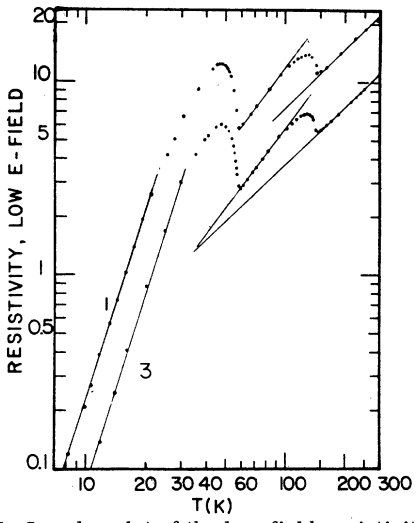

FIG. 7. Log-log plot of the low-field resistivity against temperature for two samples from different sources. The impurity scattering contribution has been subtracted out. Above T_1 (145 K) the resistivity varies as $T^{0.98}$. Above T_2 (59 K) the power law is $T^{1.40}$ and below 30 K the behavior is $T^{3.60}$. The RRR and anomaly amplitudes of both samples are given in Table I.

TABLE I. Comparison of the anomaly amplitudes with the residual-resistivity ratio (RRR) for four samples. The anomalies are identified by the transition temperature T_1, T_2 with which they are associated. Their amplitudes have been normalized as follows: $A_{\text{norm.}}(T_1) = (R_{128} - R_{145})/R_{299} - R_{4.2})$, and $A_{\text{norm.}}(T_2) = (R_{48} - R_{59})/(R_{299} - R_{4.2})$, where R_T is the sample resistance at T. The amplitude is taken to be the difference of the resistivity ρ at the two temperatures where $d\rho/dt$ vanishes. This is then normalized to the room-temperature resistivity (with the impurity contribution subtracted out). The variation is 5% (7%) for the low-(high-) temperature anomaly.

Sample	1	2	3	4
RRR	29.7	59.7	61.4	81.7
$A_{\text{norm.}}(T_1)$	0.119	0.118	0.121	0.126
$A_{\text{norm.}}(T_2)$	0.305	0.295	0.303	0.290

background, which was then subtracted from the results of the run with the sample in the cavity. Since the loss due to the sample is generally large compared to the background variation with temperature (the cavity remained at room temperature while the sample was cooled by the finger Dewar) errors due to this subtraction procedure were not significant. Altogether, microwave measurements were performed on eight samples from the Nantes batch with incident power varying from 300 nW to 3 μW. No differences from Fig. 2 were observed except for the larger scatter due to decreased sensitivity at the lowest powers.

Figure 7 shows the dc longitudinal resisitivity of two samples from different batches plotted in log-log scales (after subtracting the residual resistivity. The resistivity obeys a power-law dependence as a function of temperature in each of the three regimes separated by the two transition temperatures, T_1 and T_2. The resistivity below T_2 (59 K) varies as $T^{3.6}$ while above T_1 (145 K) it varies at $T^{0.98}$. Between T_1 and T_2 the power law appears to be $T^{1.4}$ although the data fit is less conclusive. A detailed analysis of the temperature variation of the resistivity below 1 K will be reported elsewhere.[24]

We conclude this section by briefly discussing the reproducibility of the measurements reported in this paper. As shown in Fig. 7 the resistivity profile of samples from different sources shows good reproducibility in both amplitudes and in the transition temperatures. The residual resistivity ratio (RRR) of the lower curve is 80 compared to 30 for the upper curve. Non-Ohmic measurements as represented by the plot of E_0 vs T are also similar for samples from both sources. The nonlinear I-V curves display no hysteresis when either the temperature or applied electric field is cycled. Non-Ohmic measurements were also performed with three probes instead of four with no differences in the results. Up to the highest fields applied (10 V cm^{-1}) no evidence of non-Ohmicity has been found at temperatures above 145 K. All evidence from measurements on E_0 and σ_b shows that the non-Ohmic mechanism sets in only as a result of phase transitions which occur at T_1 and T_2. This would weigh against models based on nonlinear excitations such as impact ionization, self-heating, or hot electrons which have no intrinsic correlation with the phase transitions.

The microwave measurements were performed on samples from only one batch. However, reproducibility is good from sample to sample. Recent measurements[25] on the conductivity at 100 MHz have shown resistivity profiles intermediate between the dc and 9.3-GHz results. Since the 100-MHz measurements were made in a two-probe configuration it is unlikely that the difference between the 9.3-GHz and dc results is due to probe contact problems.

We present in Table I the amplitude of the anomalies in four samples, normalized to the room-temperature resistivity after subtraction of residual resistivity. The anomaly amplitudes are measured from the minimum resistivity (close to T_1 or T_2) to the maximum resistivity. The maximum variation in the 145 K anomaly amplitude is about 7%, while the maximum variation in the 59 K anomaly is 5%. There appears to be no correlation

between sample purity as measured by RRR and anomaly size although a more systematic study is necessary to resolve this question.

IV. DISCUSSION

As mentioned in Sec. I, the phase transitions have been tentatively identified with CDW formation, although concrete evidence of superlattice formation has not been obtained to date. Here we critically review the evidence supporting the CDW model, mainly by comparison with the properties of the layered compound $2H$-$NbSe_2$, which we shall briefly discuss first. We shall see that the CDW model is not only consistent with all the experimental facts, but is capable of making a prediction which is experimentally verified.

In CDW and SDW systems of dimensionality higher than one the transition manifests itself as an anomaly in the resistivity curve. In the $1T$ polytypes[2] of the transition-metal dichalcogenides the resistivity shows a discontinuous jump at the transition temperature. In the $2H$ polytypes, however (e.g.,[26] $2H$-$NbSe_2$ and[27] $2H$-TaS_2) the CDW anomaly is a smooth bump rather similar to the anomaly occurring in Cr at the Néel temperature.[14] (In Cr the anomaly is associated with the formation of spin-density waves.) In $2H$-$NbSe_2$ both the size of the anomaly as well as the CDW transition temperature T_{CDW} decrease with hydrostatic pressure.[28] At the same time the superconducting temperature T_c increases until at 33 kbars the CDW states appears to be unstable with respect to the superconducting state, and T_c levels off at about 8 K. The decrease in T_{CDW} with pressure may be understood[28] by examining the competition between lattice strain energy and the lowering of the electronic free energy as a result of superlattice gap formation at the FS. The CDW instability occurs when the gain in electronic energy exceeds the lattice strain energy. Since pressure increases the lattice strain energy, the instability occurs at a lower temperature where the sharper Fermi-Dirac distribution increases the gain in electronic energy. The simultaneous rise in the superconducting transition temperature has been interpreted by Berthier *et al.*[28] as evidence that the CDW and superconducting states are mutually exclusive. Pressure suppresses the former, while favoring the latter. A small thermal anomaly in the specific heat has also been measured at T_{CDW} in $2H$-$NbSe_2$.[29]

In $NbSe_3$ both the transition temperatures T_1 and T_2 and the size of their associated anomalies decrease with hydrostatic pressure.[15] A large thermal anomaly[16] appears in the specific heat at T_2 (59 K) and the compound becomes superconducting only under pressure.[17] (T_c initially increases with pressure at the rate of 0.6 K/kbars.) The T_c-versus-pressure curve extrapolates to zero at about 0.2 kbars. Finally the large size of the anomalies implies that the electron gas is drastically affected by the transitions. It is unlikely that the large increase in resistivity at T_1 and T_2 comes from a change in the carrier mobilities. A more plausible explanation is that the number of carriers has been drastically reduced. This suggests that the electron gas is strongly coupled to the mechanism driving the phase transition, which is consistent with a CDW or SDW model.

At this point it is worthwhile to examine the dimensionality of the system. Despite its needle-like morphology and linear-chain crystal structure, $NbSe_3$ is probably not one-dimensional in the sense of KCP and TTF-TCNQ. Low-temperature measurements[12] on the high-field magnetoresistance show strong Shubnikov–de Haas oscillations, which are anisotropic. The oscillations reveal only one strong Fourier component despite the complicated unit cell. Furthermore, the absence of a Peierls transition to an insulating state implies that not all of the FS is affected by the CDW gap. However, the large increase in the resistivity suggests that a significant fraction of the FS is affected, i.e., the nesting criterion is satisfied by a significant fraction of the FS, compared with the case in $2H$-$NbSe_2$.

In the CDW model, the giant anomalies find a natural explanation in terms of the fraction of the FS destroyed by gap formation.[30]

The conductivity of a metal may be written[31]

$$\sigma = \frac{e^2 l}{4\pi^3 \hbar} \int_{FS} \frac{dS}{|v_k|} \frac{l_{\vec{k}}}{l} \cos^2\theta_{\vec{k}}, \tag{10}$$

where the surface integral is over the FS, $l_{\vec{k}}$ is the mean free path of an electron at $\vec{k}$, and $\theta_{\vec{k}}$ is the angle between $\vec{v}_{\vec{k}}$ and the applied electric field. For an isotropic metal $l_{\vec{k}}$ is independent of $\vec{k}$, and σ becomes directly proportional to the total FS area. In the presence of anisotropic scattering or anisotropic dispersion σ is still proportional to the total FS, suitably weighted by $l_{\vec{k}}/l$ and $\cos^2\theta_{\vec{k}}$. The formation of gaps over a fraction α of the FS has two effects: it removes the contribution of fraction α from the integral, and $\cos^2\theta_{\vec{k}}$ is altered for $\vec{k}$ immediately adjacent to the gap. The second effect is usually much smaller than the first. If we assume that all the pre-transition temperature dependence of $\sigma(T)$ resides in $l(T)$, then the shapes of the two anomalies may be understood as arising from the gradual transition from metallic behavior with the original (weighted) FS area to metallic behavior with progressively smaller FS's as the transitions at T_1 and T_2 destroy portions of the FS. This is consistent with the log-log plot of the re-

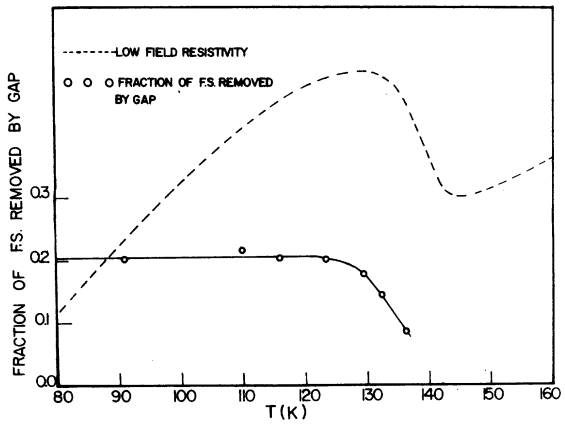

FIG. 8. Parameter α_1 (open circles) define by Eqs. (4) and (11) vs temperature. In the text α_1 is interpreted as the fraction of Fermi surface destroyed by the CDW gap which develops at 145 K. Below 122 K, α_1 becomes *temperature independent* and the low-field resistivity (broken line) resumes metallic behavior.

sistivity in Fig. 7. Calling α_1 (α_2) the fraction of the FS destroyed by the transition at T_1 (T_2) we have two possibilities for its temperature variation. If α_1 jumps abruptly to its maximum value as the temperature crosses T_1, the resistivity should show a discontinuous break. Since the growth of both anomalies is rather gradual our model predicts that α increases smoothly from zero as the temperature crosses T_1 (or T_2). When α stops increasing the resistivity reaches its maximum value, and then resumes its metallic behavior. As mentioned in the Introduction the non-Ohmic data provide a direct measurement of the fractions α_1, α_2 as a function of temperature. Deferring for the moment discussions on the mechanism responsibile for the non-Ohmicity we see that the empirically-derived relation [Eq. (1)] for the non-Ohmic data enables us to extrapolate the non-Ohmic effect to infinite E fields. If we make the assumption that in the limit of infinite field we recover the conductivity appropriate to the FS at temperatures above the phase transition, then the parameter α defined by Eq. (4) may be expressed as [using Eq. (10) in Eq. (4)]:

$$1-\alpha_1(T)=\int_{\mathrm{FS}(T)} dS\, A_{\vec{k}} \Big/ \int_{\mathrm{FS}(T')} dS\, A_{\vec{k}} \ , \qquad (11)$$

with

$$A_{\vec{k}}=(l_{\vec{k}}/l)\cos^2\theta_{\vec{k}} \ . \qquad (12)$$

In Eq. (11) T is a temperature between T_1 and T_2 and T' is a temperature above T_1. The integral in the numerator is over the portion of the FS not affected by the gap, and the integral in the denominator is over the whole FS before the gap forms. Thus α_1 gives approximately the fraction of weighted FS destroyed by the gap which develops at T_1. The identification of α_1 is only approximate because gap formation may affect $\cos^2\theta_{\vec{k}}$ for $\vec{k}$ immediately adjacent to the gap. Since σ_a and σ_b are measurable quantities, α is experimentally accessible. Figure 8 shows a plot of α_1 within the high-temperature anomaly. As expected, α_1 grows smoothly from zero to its maximum value of 0.20 and *remains temperature independent*, while the low-field resistivity $1/\sigma_a$ resumes its metallic behavior. Approximately twenty percent of the FS is destroyed by the 145-K transition. As the temperature crosses T_2 new gaps develop over the remaining 80% of the FS. We may repeat the same analysis to obtain α_2 provided we modify our limiting process to obtain σ_{b2}. At T_2 (59 K) the 145-K gap and α_1 have reached their maximum value (assuming a BCS-type gap equation). Whatever the non-Ohmic mechanism, it is certainly possible that at extremely high electric fields we will continue to observe breakdown effects due to the 145-K transition even at temperatures below T_2 (59 K). This would complicate the analysis of the non-Ohmic data below T_2, and a simple interpretation such as that which led to Eq. (11) would not be possible. However, if we restrict ourselves to fields below which breakdown effects due to the 145-K transition are absent, then α_2 may again be defined as in Eq. (4) with σ_{b2} defined by Eq. (3) where it is understood that in the "infinite" limit the field strength is still less than that necessary to observe breakdown contributions from the 145-K transition. Fortunately, in practice this condition poses no problem because E_{02} (the activation field below T_2) is an order of magnitude smaller than E_{01}. At 59 K E_{01} is approximately 3.5 V cm^{-1} and decreasing. Thus the breakdown contributions from the two anomalies separate into two well-defined regimes. Figure 9 shows the plot of α_2 vs temperature. It shows a behavior similar to α_1. In the same figure we have plotted the high-field limit resistivity defined by

$$\rho_\infty(T)=[\sigma_a(T)+\sigma_b(T)]^{-1} \ . \qquad (13)$$

ρ_∞ shows a vestigial structure near 59 K. This could be due to the modification of the $\cos^2\theta_{\vec{k}}$ factor in Eq. (10) as discussed in the text following that equation. From the data we conclude that 62% of the *remaining* FS is destroyed by gaps that develop at 59 K. As expected this accounts for the larger amplitude of the lower-temperature anomaly.

We have deferred discussion on the non-Ohmic mechanism and the microwave data because they are the most difficult to account for as well as the most interesting. The field dependence of the con-

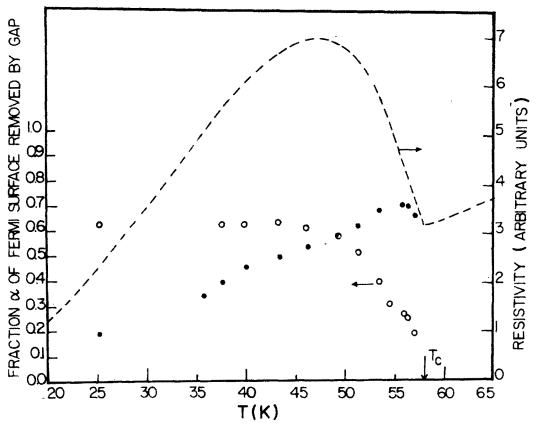

FIG. 9. Behavior of α_2 (open circles) defined by Eq. (4) vs temperature. The resistivity in the high-field limit (solid circles) shows a structure near 59 K. The low-field resistivity (broken line) is displayed for comparison. As in the high-temperature transition, α_2 increases from zero with decreasing temperature. When α_2 attains its constant value (below 45 K), the low-field resistivity resumes its metallic behavior.

ductivity in Eq. (1) is characteristic of quantum tunneling processes induced by an applied electric field. The prototype process is Zener's[32] original proposal that a high field can cause tunneling of carriers across energy gaps in k space. The Zener tunneling current I^Z (per unit volume of semiconductor) has been derived by Kane[33] as

$$I^Z = (e^3E^2m_r^{1/2}/18\pi\hbar\Delta^{1/2})e^{-E_0^Z/E}, \tag{14}$$

with

$$E_0^Z = m^{1/2}\Delta^{3/2}/2\hbar e = \pi\Delta^2/2\hbar ev, \tag{15}$$

and

$$m_r = \Delta/v^2. \tag{16}$$

In Eqs. (14)–(16), Δ is the gap across which tunneling occurs, v is the Fermi velocity of carriers in the absence of the gap, m_r is a reduced mass, and e is the electronic charge. Our initial attempt was to identify the non-Ohmic breakdown with Zener tunneling across the CDW gaps. This would have provided further evidence of gap formation at the FS. However, putting an upper limit of 10^8 cm sec^{-1} for v in Eq. (15) we obtained an upper limit of 6.1×10^{-5} eV for Δ_2 at 50 K and 2.4×10^{-4} eV for Δ_1 at 115 K (where E_{02} and E_{01} attain their minimum value). The thermal fluctuation energy kT at these temperatures is 4.3×10^{-3} eV (at 50 K) and 9.97×10^{-3} eV (at 115 K). Thus using conventional Zener tunneling equations as given by Eqs. (14) and (15) we are confronted with "gap" values one to two orders of magnitude smaller than the thermal fluctuation. Another serious difficulty with the Zener model is the temperature dependence of E_0. According to Eq. (15) E_0^Z varies as Δ^2 which should increase as $1 - T/T_c$ near T_c using mean-field results. This is not what is observed at either transition.

The microwave resistivity shows substantial disagreement with the dc results below 145 K. This is unexpected from a simple Drude-type analysis of the ac conductivity, which gives a significant difference between ac and dc conductivity only when $\omega\tau > 1$, where ω is the ac angular frequency and τ the single-particle lifetime. Assuming a τ of 10^{-13} sec, then $\omega\tau$ equals 5×10^{-3} GHz. Clearly a single-particle model fails to explain the discrepancy. A plausible solution is to postulate that very small gaps exist which drastically affect the dc transport, but are ineffective at microwave frequencies since the carriers can be excited across the gaps by absorbing a 9.3-GHz photon of energy $\hbar\omega \simeq 10^{-5}$ eV. However, we have seen that such small gaps are highly unlikely to have much effect on transport measurements at temperatures as high as T_1 and T_2.

The difficulties with the Zener tunneling picture and the impossibility of incorporating the microwave data into a single-particle theory reopen the question of the nature of the phase transitions at T_1 and T_2 and their effect on the transport properties. We briefly discuss two alternative models not based on CDW formation, which have the merit of fitting some of the observed data. However, it will be seen that these alternatives encounter serious difficulties of their own and, unlike the CDW model, are not useful in making predictions which can be experimentally verified. Finally, we return to the CDW model and explore on a speculative basis various exotic mechanisms which may reconcile the model with the non-Ohmic and microwave experiments.

The first alternative, the interrupted-strand model, ascribes the resistivity anomalies to breaks in the current paths, which are assumed to be filamentary. These breaks appear below each transition temperature. The application of high electric fields induces quantum tunneling across barriers resulting in a field-dependent current similar to Eq. (14). Since these barriers are in real space with widths which may be less than 1 μm, the fields across them will be orders of magnitude larger than those across the sample. Hence we do not encounter the problem of gap energies orders of magnitude smaller than kT. The microwave resistivity will not be affected by the barriers, provided the RC time constant is sufficiently long (where R and C are the equivalent resistance and capacitance of the filaments and barriers). Hence we expect anomalies much reduced in size at high

frequencies. The weakness of this model is its selectivity in fitting some of the experiments while ignoring others. The data on the temperature dependence of α_1 and α_2, for example, do not find a natural explanation within this model. Also, because of its *ad hoc* and phenomenological basis, it leaves unexplained the microscopic nature of the strand interruptions and their connection with the transition temperature. Indeed the postulated statistical nature of the random breaks would seem inconsistent with the reproducibility of the amplitudes of the anomalies from run to run, and from sample to sample.

A second alternative is to identify the anomalies at T_1 and T_2 with ferroelectric transitions. The dependence of T_1 and T_2 on applied pressure in $NbSe_3$ is also consistent with a structural transformation which is driven by a lattice soft mode, as in a ferroelectric material.[34] In KH_2PO_4,[35] for example, the transition temperature decreases linearly with pressure. The lattice optical-mode softening may be described by the equation[36,37]

$$\omega_{TO}^2 = A(T - T_c), \tag{17}$$

where ω_{TO} is the mode frequency and T_c the transition temperature. As $T \to T_c$, ω_{TO} decreases to zero, and the lattice undergoes a structural transformation which results in a polarization of the solid. In ferroelectric metals[34] such as the tungsten bronzes and Nb_3Sn the resulting spontaneous polarization may be difficult to detect because of screening by the conduction electrons. Application of pressure decreases T_c because the increase in strain energy stiffens the softening mode, and postpones the transition. The existence of different directions of polarization leads to domain walls, which may be made to move by the application of electric fields. Miller and Savage[38] have shown experimentally that the wall velocities vary with applied field as

$$v(E) = v_\infty e^{-E_0/E} \tag{18}$$

for low and moderate fields. The theoretical explanation[39] of Eq. (18) is not satisfactory at present. Although the similarity between Eqs. (1) and (18) is suggestive, the physical implications must be viewed with caution. Equation (18) describes the irreversible expansion of a region of polarization, whereas Eq. (1) describes the excitation and propagation of charged entities which contribute to the current. The overall evidence for the ferroelectric model appears to be much weaker than for the other two models. Much the same criticisms that were directed at the defect model are applicable to the ferroelectric model. The large size of the anomalies implies a drastic change in the number of carriers at the phase transitions. It is difficult to understand how the electron gas can be so greatly perturbed by a structural phase transition which involves the lattice alone. Superlattice Bragg planes will appear as a result of the new periodicity, but these will not bear any geometrical relationship to the FS, and the effect on the electron transport properties will be slight. In the case of the CDW model, however, the structural transformation is driven by the electron gas-photon coupling, and the superlattice Bragg planes will be located precisely over large portions of the FS. Indeed, the condition that large portions of the FS can be made to "nest"[40] by a single spanning vector is necessary for the CDW state to be stable. Thus the drastic carrier-number reduction receives the most natural explanation in the CDW model. Moreover, as has been shown, by reasoning along these lines we can extract the parameter α from the non-Ohmic data which describes the continuous decrease in free carrier concentration or FS area.

Having argued for a CDW interpretation of the transitions we may now inquire if the electric breakdown and microwave-frequency results can be accomodated in the CDW model. In the context of one-dimensional metals the possibility of observing non-Ohmic behavor in the conductivity has been discussed by many workers. In particular, Rice *et al.*[41] suggested the possibility of moving by an applied E field a condensed CDW that is pinned by impurities or lattice commensurability. Recently Rice, Bishop, Krumhansl, and Trullinger[42] have proposed a new charge-carrying excitation—ϕ particles—in a one-dimensional pinned CDW. These excitations are phase domain walls (solitons) between regions of the CDW which differ in phase by 2π. In the classical regime they have been shown[43] to be stable and to behave like classical particles. K. Maki[44] has studied the pair-creation of solitons by an applied electric field in a one-dimensional CDW and has derived the field-dependent conductivity given by

$$\sigma = \sigma_1 e^{-E_0/E}, \tag{19}$$

$$E_0 = U_\phi^2/\hbar c_0 e^*, \tag{20}$$

where E is the applied field, U_ϕ the rest energy of a solition, $\hbar$ is Planck's constant divided by 2π, c_0 is the "relativistic" velocity of the soliton, and e^* the effective charge.

The similarity between Maki's result Eq. (19) and the observed non-Ohmic conductivity in $NbSe_3$ given by Eq. (1) is highly suggestive. However, many difficulties appear in a comparison of the theory with the experimental parameters. For example, the rest energy U_ϕ as given by Eq. (20) is still two orders of magnitude lower than kT (as-

suming reasonable numbers for c_0 and e^*), and the temperature dependence of E_0 as given in Eq. (20) does not agree with experiment. Since Maki's calculations are preliminary, it may be possible to resolve these difficulties in a more refined model. Within the confines of a CDW model other mechanisms for non-Ohmic transport are possible. If the pinning of the CDW is weak, an applied electric field may depin the CDW, leading to a non-Ohmic contribution to the conductivity. A weak pinning potential implies a very low pinning frequency. This is consistent with the microwave response of the system. Lee, Rice, and Anderson[45] (LRS) have proposed that in the presence of dilute impurities a CDW may adjust its periodicity slightly to sit in the minimum of each impurity potential. In a one-dimensional solid the dc conductivity vanishes at $T=0$ K, but the ac conductivity will be large at low frequencies. LRA speculate that the mechanism may be similar to stick-slip friction, with strong nonlinearities in the conduction process. This picture may be generalized to higher dimensions. In our case only a fraction α of the FS is affected by the "sticking" of the CDW to impurities. This leads to the finite rise in the resistivity. The application of an ac field with frequency close to the pinning frequency may excite a collective mode in which segments of the pinned CDW oscillate about their pinning centers. It is possible that the pretransition resistivity profile may be recovered at an appropriate frequency. This may explain the complete absence of the anomaly at 59 K in the 9.3-GHz data. In the absence of more direct evidence these comments must remain speculative.

V. CONCLUSION

We have presented results of transport measurements at dc and microwave frequency on the linear-chain metal $NbSe_3$, which undergoes two transitions at 145 and 59 K. The conductivity is anomalous in that relatively weak electric fields can cause a nonlinear I-V characteristic within the resistivity anomalies, and in that relatively low-frequency ac measurements on the resistivity show strikingly different results from dc. The non-Ohmic data can be fitted to the analytic expression Eq. (1) at all investigated temperatures below 145 K. The phase transitions have been tentatively identified with CDW formation on the basis of a comparison with the layered compound $2H$-$NbSe_2$. On the basis of the CDW model we have argued that the anomalies result from the continuous destruction of portions of the FS by CDW formation, and have obtained experimental verification of this hypothesis. To explain the non-Ohmic behavior as well as the microwave result we briefly discussed the Zener-tunneling model, the defect model, and the ferroelectric model, and concluded that these models were incapable of offering a unified, consistent theory for the results presented here. In conjunction with results published elsewhere the CDW model appears to present the strongest case. This suggests that the non-Ohmicity and anomalous microwave response result from the electrodynamics of excitations in pinned CDWs. Finally we speculated on various possibilities such as soliton excitation and CDW depinning by electric fields.

ACKNOWLEDGMENTS

It is a pleasure to acknowledge stimulating discussions with M. H. Cohen, L. M. Falicov, J. Lajzerowicz, Patrick Lee, A. Madhukar, K. Maki, A. M. Portis, and S. Trullinger. We wish to express our gratitude to J. Rouxel and to J. Savage for providing samples of $NbSe_3$.

---

†Supported in part by NSF through the Division of Materials Research, Grant No. 75-23018.

*Present address.

‡Permanent address: Centre de Recherches sur les Tres Basses Temperatures, B. P. 166, 38042, Grenoble-Cedex, France.

[1]For a review see J. A. Wilson, F. J. Di Salvo, and S. Mahajan, Adv. Phys. 24, 117 (1975).

[2]For a review, see *One Dimensional Conductors*, edited by H. G. Shuster (Springer-Verlag, Berlin, 1975).

[3]R. Peierls, *Quantum Theory of Solids* (Oxford U.P., London, 1955), Chap. 5; M. J. Rice and S. Strassler, Solid State Commun. 13, 125 (1973).

[4]J. A. Wilson, F. J. Di Salvo, and S. Mahajan, Phys. Rev. Lett. 32, 882 (1974); P. M. Williams, G. S. Parry, and C. B. Scrubby, Philos. Mag. 29, 695 (1974).

[5]R. Comes, M. Lambert, H. Launois, and H. R. Zeller, Phys. Rev. B 8, 571 (1973).

[6]F. Denoyer, F. Comes, A. F. Garito, and A. J. Heeger, Phys. Rev. Lett. 35, 445 (1975); H. A. Mook and C. R. Watson, Jr., *ibid.* 36, 801 (1976).

[7]References to the TTF-TCNQ literature are given in G. A. Thomas *et al.*, Phys. Rev. B 13, 5105 (1976); M. J. Cohen, L. B. Coleman, A. F. Garito, and A. J. Heeger, *ibid.* 13, 5111 (1976). A recent review appears in A. J. Berlinsky, Contemp. Phys. 17, 331 (1976).

[8]M. J. Cohen, P. R. Newman, and A. J. Heeger, Phys. Rev. Lett. 37, 1500 (1976).

[9]P. Monceau, N. P. Ong, A. M. Portis, A. Meerschaut, and J. Rouxel, Phys. Rev. Lett. 37, 602 (1976).

[10]N. P. Ong and P. Monceau, Bull. Am. Phys. Soc. 22, 454 (1977).

[11]A. Meerschaut and J. Rouxel, J. Less Common Metals 39, 197 (1975).

[12]P. Monceau, Solid State Commun. (to be published); R. M. Fleming and R. V. Coleman, Bull. Am. Phys.

Soc. 22, 281 (1977).
[13]P. Haen, P. Monceau, B. Tissier, G. Waysand, A. Meerschaut, P. Molinie, and J. Rouxel, *Proceedings Fourteenth International Conference on Low Temperature Physics* (Otaniami, Finland, 1975), Vol. 5, p. 445.
[14]A. L. Trego and A. R. Mackintosh, Phys. Rev. 166, 495 (1968).
[15]P. Haen, G. Waysand, G. Boch, A. Waintal, P. Monceau, N. P. Ong, and A. M. Portis, J. Phys. (Paris) 37, C4-179 (1976).
[16]J. Chaussy, P. Haen, J. C. Lasjaunias, P. Monceau, G. Waysand, A. Waintal, A. Meerschaut, P. Molinie and J. Rouxel, Solid State Commun. 20, 759 (1976).
[17]P. Monceau, J. Peyard, and J. Richard, Bull. Am. Phys. Soc. 22, 403 (1977); P. Monceau, J. Peyard, J. Richard, and P. Molinié, Phys. Rev. Lett. 39, 160 (1977).
[18]Details of the experiments are given in N. P. Ong, thesis (University of California, Berkeley, 1976) (unpublished).
[19]L. I. Buranov and I. F. Shchegolev, Prib. Tekh. Eksp. 2, 171 (1971).
[20]S. K. Khanna, E. Ehrenfreund, A. F. Garito, and A. J. Heeger, Phys. Rev. B 10, 2205 (1974).
[21]N. P. Ong, J. Appl. Phys. 48, 2935 (1977).
[22]M. Cohen, S. K. Khanna, W. J. Gunning, A. F. Garito, and A. J. Heeger, Solid State Commun. 17, 367 (1975).
[23]We are indebted to A. M. Portis for suggesting this approach.
[24]P. Haen and P. Monceau (unpublished).
[25]S. W. Longcor and A. M. Portis (private communication).
[26]D. J. Huntley and R. F. Frindt, Can. J. Phys. 52, 861 (1974).
[27]J. P. Tidman, O. Singh, A. E. Curzon, and R. F. Frindt, Philos. Mag. 30, 1191 (1975).
[28]C. Berthier, P. Molinié, and D. Jerome, Solid State Commun. 18, 1393 (1976); R. Delaplace, P. Molinie, and D. Jerome, J. Phys. Lett. (Paris) 37, L-13 (1976).
[29]J. M. E. Harper, T. H. Geballe, and F. J. Di Salvo, Phys. Lett. A 54, 27 (1975).
[30]This analysis was first suggested to us by Leo Falicov.
[31]See, for example, J. M. Ziman, *Electrons and Phonons* (Clarendon, London, 1960), p. 262.
[32]C. Zener, Proc. R. Soc. Lond. A 145, 523 (1934); an elementary treatment is given by J. M. Ziman, *Principles of the Theory of Solids*, 2nd ed. (Cambridge University, Cambridge, England, 1972), Sec. 6.8.
[33]E. O. Kane, J. Phys. Chem. Solids 12, 181 (1959).
[34]A review is given by J. F. Scott, Rev. Mod. Phys. 46, 83 (1974).
[35]G. A. Samara, Phys. Rev. Lett. 27, 103 (1971).
[36]W. Cochran, Phys. Rev. Lett. 3, 521 (1959); Adv. Phys. 9, 387 (1960); 10, 401 (1961).
[37]A review is given by A. S. Barker, Jr., in *Far Infrared Properties of Solids*, edited by S. S. Mitra and S. Nudelman (Plenum, New York, 1970), p. 247.
[38]R. C. Miller and A. Savage, Phys. Rev. 115, 1176 (1959).
[39]R. C. Miller, G. Weinreich, Phys. Rev. 117, 1460 (1960).
[40]W. M. Lomer, Proc. Phys. Soc. Lond. 80, 489 (1962).
[41]M. J. Rice, S. Strassler, and W. R. Scheider, in *One-Dimensional Conductors*, edited by H. G. Schuster (Springer-Verlag, Berlin, 1975), Chap. 19.
[42]M. J. Rice, A. R. Bishop, J. A. Krumhansl, and S. E. Trullinger, Phys. Rev. Lett. 36, 432 (1976).
[43]M. B. Fogel, S. E. Trullinger, A. R. Bishop, and J. A. Krumhansl, Phys. Rev. Lett. 36, 1411 (1976).
[44]Kazumi Maki, Phys. Rev. Lett. 39, 46 (1977).
[45]P. A. Lee, T. M. Rice, and P. W. Anderson, Solid State Commun. 14, 703 (1974).